

Fragmentation cross sections of Fe^{26+} , Si^{14+} and C^{6+} ions of $0.3 \div 10$ A GeV on polyethylene, CR39 and aluminum targets

S. Cecchini¹, T. Chiarusi¹, G. Giacomelli¹, M. Giorgini¹, A. Kumar^{1,4}, G. Mandrioli¹, S. Manzoor^{1,2,3}, A. R. Margiotta¹, E. Medinaceli¹, L. Patrizii¹, V. Popa^{1,5}, I. E. Qureshi^{2,3}, G. Sirri¹, M. Spurio¹ and V. Togo¹

1. *Phys. Dept. of the University of Bologna and INFN, Sezione di Bologna, Viale C. Berti Pichat 6/2, I-40127 Bologna, Italy*

2. *PD, PINSTECH, P.O. Nilore, Islamabad, Pakistan*

3. *COMSATS Institute of Information Technology 30, H/8-1, Islamabad, Pakistan*

4. *Dept. Of Physics, Sant Longowal Institute of Eng. and Tech., Longowal 148 106, India*

5. *Institute of Space Sciences, Bucharest R-077125, Romania*

Abstract. We present new measurements of the total and partial fragmentation cross sections in the energy range $0.3 \div 10$ A GeV of ^{56}Fe , ^{28}Si and ^{12}C beams on polyethylene, CR39 and aluminum targets. The exposures were made at BNL, USA and HIMAC, Japan. The CR39 nuclear track detectors were used to identify the incident and survived beams and their fragments. The total fragmentation cross sections for all targets are almost energy independent while they depend on the target mass. The measured partial fragmentation cross sections are also discussed.

1 Introduction

The interaction and propagation of intermediate and high energy heavy ions in matter is a subject of interest in the fields of astrophysics, radio-biology and radiation protection [1]. An accurate description of the fragmentation of heavy ions is important to understand the effects of the high Z component of Cosmic Rays (CRs) on humans in space [2] and for shielding in space and in accelerator environments. More recently the interaction and transport of light energetic ions in tissue-like matter became of particular interest in medicine and for hadron therapy of cancer [3].

When a heavy ion impinges on a target, it undergoes fragmentation processes depending on the impact parameter between the colliding nuclei. The target fragments carry little momentum. At high energies, the projectile fragments travel at nearly the same velocity as the beam ions and have only a small deflection.

The availability of heavy ion beams at the CERN SPS, at BNL (USA) and at the HIMAC (Japan) facilities made possible to investigate the projectile fragmentation on different targets and for different projectile energies. Several authors [4-10] have successfully used Nuclear Track Detectors (NTD's) for systematic measurements of nuclear fragmentation cross sections.

The present study is focused on Fe, Si and C ion interactions in CH_2 , CR39 ($\text{C}_{12}\text{H}_{18}\text{O}_7$)_n and Al targets. We used CR39 detectors, which are sensitive for a wide range of charges down to $Z = 6e$ in the relativistic energy region [4, 11]. NTD's have been used to search for exotic particles like Magnetic Monopoles and Nuclearites [12, 13], to study cosmic ray composition [14] and for environmental studies [15].

2 Experimental Procedure

Stacks composed of several CR39 NTD's, of size $11.5 \times 11.5 \text{ cm}^2$, and of different targets were exposed to 0.3, 1, 3, 5 and 10 A GeV Fe^{26+} , 1, 3, 5 A GeV Si^{14+} ions at BNL, 0.41 A GeV Fe^{26+} , 0.29 A GeV C^{6+} ions at HIMAC. For these exposures we used the geometry sketched in Fig. 1: three and four CR39 sheets, $\sim 0.7 \text{ mm}$ thick, were placed before and after the target, respectively. The exposures were done at normal incidence, with a density of $\sim 2000 \text{ ions/cm}^2$. After exposures the CR39 foils were etched in 6N NaOH aqueous solution at 70°C for 30 h (in two steps 15h+15h) in a thermostatic water bath with constant stirring of the solution. After etching, the beam ions and their fragments manifest in the CR39 NTD's as etch pit cones on both sides of each detector foil.

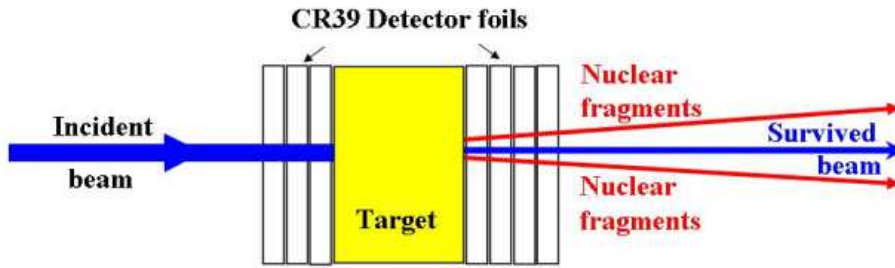


Figure 1: Sketch of the target-detector configuration used for the exposures to different ion beams.

The base areas of the etch-pit cones (“tracks”), their eccentricity and central brightness were measured with an automatic image analyzer system [16] which also provides their absolute coordinates. A tracking procedure was used to reconstruct the path of beam ions through the front faces of the detector upstream (with respect to the target) foils; a similar tracking procedure was performed through the three measured front faces of downstream CR39 detectors. The average track base area was computed for each reconstructed ion path by requiring the existence of signals in at least two out of three sheets of the detectors. In Fig. 2a,b the average base area distributions for 1 A GeV Si^{14+} and 1 A GeV Fe^{26+} beam ions and their fragments after the CH_2 targets are shown.

3 Total fragmentation cross sections

The numbers of incident and survived beam ions were determined considering the mean area distributions of the beam peaks before and after the target and evaluating the integral of the gaussian fit of the beam peaks.

The total charge changing cross sections were determined with the survival fraction of ions using the following relation

$$\sigma_{tot} = \frac{A_T \ln(N_{in}/N_{out})}{\rho t N_{Av}} \quad (1)$$

where A_T is the nuclear mass of the target (average nuclear mass in case of polymers: $A_{CH_2} = 4.7$, $A_{CR39} = 7.4$); N_{in} and N_{out} are the numbers of incident ions before and after the target, respectively; ρ (g/cm^3) is the target density; t (cm) is the thickness of the target and N_{Av} is Avogadro number.

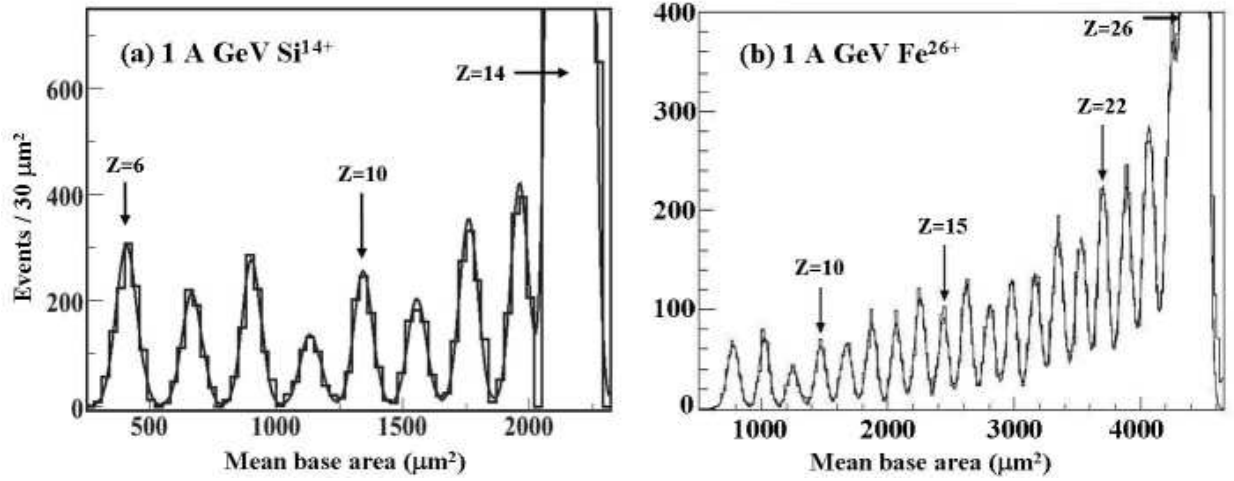


Figure 2: Distributions of the average base areas for tracks present in at least 2 out of 3 measured CR39 sheets located after the CH₂ target. The data concern (a) 1 A GeV Si¹⁴⁺ and (b) 1 A GeV Fe²⁶⁺ ions. Each peak has a gaussian shape with $\sigma \sim 0.2e$. Notice that the peaks with Z even are generally higher than the close by peaks with Z odd.

Systematic uncertainties in σ_{tot} were estimated to be smaller than 10%: contributions arise from the measurements of the density and thickness of the targets, from the separation of the beam peak from the $\Delta Z = Z_{fragment} - Z_{beam} = -1$ fragments (Fig. 2), from fragmentation in the CR39 foils and from the tracking procedure.

The measured total charge changing cross sections are given in the 4th column of Table 1. Fig. 3a shows the total cross sections of Fe²⁶⁺ projectiles at various beam energies on the CH₂ and Al targets. Our results for Si¹⁴⁺ and C⁶⁺ projectiles are given in Table 2 and are plotted vs energy in Fig. 3b.

The total cross sections are almost energy independent, in agreement with the data from other authors [6, 7, 8, 9].

Various theoretical models/formulae for the total fragmentation cross sections were proposed and fitted to the experimental data with different geometrical radii and overlapping parameters [5]. In Fig. 3 our data are compared with the semi-empirical formula [17] for nuclear cross sections (solid lines)

$$\sigma_{tot} = \pi r_0^2 (A_P^{1/3} + A_T^{1/3} - b_0)^2 \quad (2)$$

where $r_0 = 1.31$ fm, $b_0 = 1.0$, A_P and A_T are the projectile and target mass numbers, respectively. Various authors used different values for the overlap parameter b_0 within the interval $0.74 \div 1.3$ [5-10].

Figs. 4a,b show the total fragmentation cross sections vs target mass number A_T for Fe²⁶⁺, Si¹⁴⁺ and C⁶⁺ beams of various energies. The solid lines are the predictions of Eq. 2, to which we added the electromagnetic dissociation contribution, $\sigma_{EMD} = \alpha Z_T^\delta$, with $\alpha = 1.57$ fm² and $\delta = 1.9$ [last ref. of [4]]. The total fragmentation cross sections increase with increasing target mass number. Part of the increase is due to the effect of electromagnetic dissociation.

The data from other authors [6, 7, 9, 10] are plotted for comparison and show good agreement with our data, within the experimental uncertainties.

Energy (A GeV)	Target	A_T	σ_{tot} (mb)
10	CH ₂	4.7	1147 \pm 97
10	CR39	7.4	1105 \pm 360
5	CH ₂	4.7	1041 \pm 130
5	CR39	7.4	1170 \pm 470
3	CH ₂	4.7	904 \pm 140
3	CR39	7.4	1166 \pm 67
1	CH ₂	4.7	1105 \pm 60
1	CR39	7.4	1113 \pm 176
1	Al	27	1870 \pm 131
0.41	CH ₂	4.7	948 \pm 54
0.41	CR39	7.4	1285 \pm 245
0.41	Al	27	1950 \pm 126
0.30	CH ₂	4.7	949 \pm 61
0.30	CR39	7.4	1174 \pm 192
0.30	Al	27	2008 \pm 144

Table 1: Measured total fragmentation cross sections, with statistical standard deviations, for Fe²⁶⁺ ions of different energies (col. 1) on different targets (col. 2).

Si ¹⁴⁺ ions			C ⁶⁺ ions		
Energy (A GeV)	Target	σ_{tot} (mb)	Energy (A GeV)	Target	σ_{tot} (mb)
5	CH ₂	757 \pm 168	0.29	CH ₂	460 \pm 53
3	Al	1533 \pm 133	0.29	CR39	513 \pm 52
1	CR39	1113 \pm 176	0.29	Al	1155 \pm 108
1	H	483 \pm 76			
1	CH ₂	694 \pm 70			
1	C	1117 \pm 62			
1	Al	1397 \pm 138			

Table 2: Measured total fragmentation cross sections σ_{tot} for Si¹⁴⁺ ions of different energies (col.1) on different targets (col. 2) and for 0.29 A GeV C⁶⁺ ions on different targets (col. 5). Errors are statistical standard deviations.

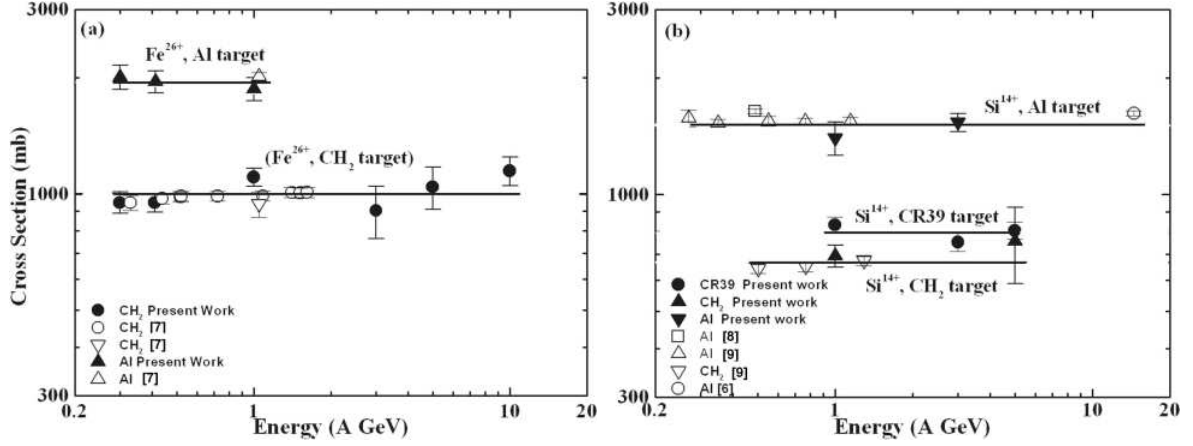


Figure 3: Total fragmentation cross sections for (a) Fe ions of different energies in CH_2 and Al targets and (b) for Si ions in CH_2 , CR39 and Al targets. For comparison the measured cross sections from refs. [6, 7, 8, 9] are also shown, together with the predictions from Eq. 2.

4 Partial fragmentation charge changing cross sections

If the thickness of the target is small compared to the mean free path of the fragments in that material, the partial fragmentation cross sections can be calculated using the simple relation

$$\sigma(Z_i, Z_f) \simeq \frac{1}{Kt} \frac{N_f}{N_i} \quad (3)$$

where $\sigma(Z_i, Z_f)$ is the partial fragmentation cross section of an ion Z_i into the fragment Z_f , K is the number of target nuclei per cm^3 , t is the thickness of the target, N_i is the number of survived ions after the target and N_f is the number of fragments produced with charge Z_f . This expression may be valid also for a thick target, assuming that the number of fragments before the target is zero.

For the Fe ions, we observed that fragments are present even before the targets. In this case the partial charge change cross sections have been computed via the relation

$$\sigma_{\Delta Z} = \frac{1}{Kt} \left(\frac{N_{out}^f}{N_s^p} - \frac{N_{in}^f}{N_{in}^p} \right) \quad (4)$$

where N_{in}^f and N_{out}^f are the numbers of fragments of each charge before and after the target, and N_{in}^p and N_s^p are the numbers of incident and survived projectile ions.

The distributions, after the CH_2 targets, of the fragments for 1 A GeV Si^{14+} and 1 A GeV Fe^{26+} ions are shown in Figs. 2a,b. The relative partial fragmentation cross sections for $\Delta Z = -1, -2, -3, \dots, -18$ are given in Table 3. The quoted errors are statistical standard deviations; systematic uncertainties are estimated to be about 10%. A clear odd-even effect is visible in Fig. 2: the cross sections for the Z -even fragments are generally larger than those for the Z -odd fragments close by.

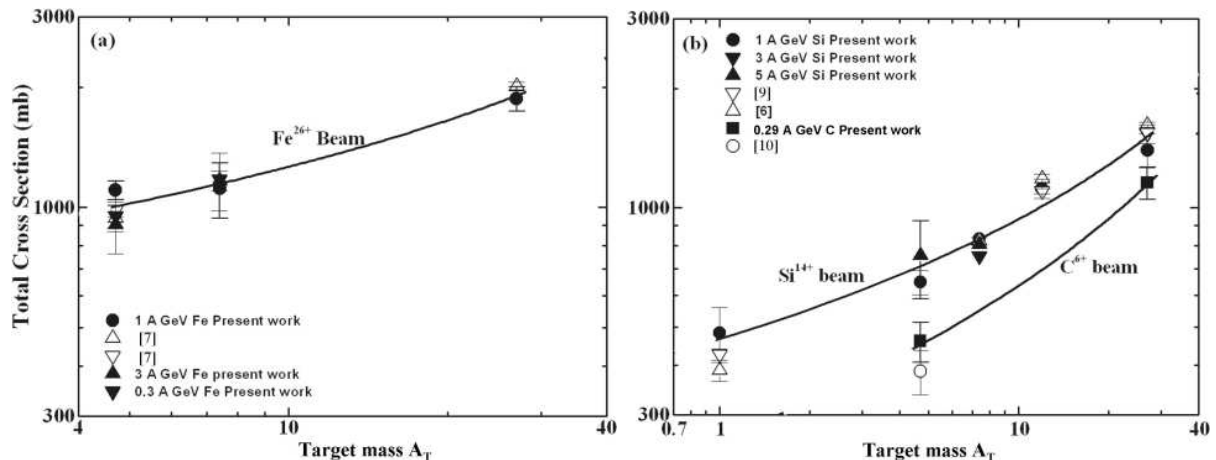


Figure 4: Dependence of the total fragmentation cross sections on the target mass (a) for Fe ions and (b) for Si and C ions. For comparison the measured cross sections from refs. [6, 7, 9, 10] are also shown. The solid lines are from Eq. 2 corrected by the σ_{EMD} term.

5 Conclusions

The total fragmentation cross sections for ^{56}Fe , ^{28}Si and ^{12}C ion beams of $0.3 \div 10$ A GeV energies on polyethylene, CR39 and aluminum targets were measured using CR39 NTD's [18].

The total cross sections for all the targets and energies used in the present work do not show any observable energy dependence. There is a dependence on target mass; the highest cross sections are observed for Al targets and this is mainly due to the contribution of electromagnetic dissociation. The present data of total fragmentation cross sections are in agreement with similar experimental data in the literature [4-10].

The presence of well separated fragment peaks, see Fig. 2, allowed the determination of the partial fragmentation cross sections. On the average the partial cross sections decrease as the charge change ΔZ increases. The data in Fig. 2 and the partial cross sections in Table 3 indicate a clear Z odd-even effect.

The measured cross section data indicate that passive NTD's, specifically CR39, can be used effectively for studies of the total and partial charge changing cross sections, also in comparison with active detectors.

Acknowledgments

This work was in part financed by the MIUR PRIN 2004 Program (ex 40%), Prot. 2004021217.

We thank the technical staff of BNL and HIMAC for their kind cooperation during the beam exposures. We acknowledge the contribution of our technical staff, in particular of A. Casoni, M. Errico, R. Giacomelli, G. Grandi and C. Valieri. We thank INFN and ICTP for providing fellowships and grants to non-Italian citizens.

References

- [1] C. X. Chen et al., Phys. Rev. C49 (1994) 3200.

ΔZ	1 A GeV Fe ²⁶⁺	1 A GeV Si ¹⁴⁺
-1	-	293 \pm 18
-2	338 \pm 11	177 \pm 12
-3	285 \pm 11	123 \pm 11
-4	252 \pm 10	122 \pm 11
-5	249 \pm 10	62 \pm 8
-6	197 \pm 9	117 \pm 11
-7	168 \pm 8	83 \pm 9
-8	132 \pm 7	90 \pm 10
-9	175 \pm 8	
-10	107 \pm 7	
-11	152 \pm 6	
-12	105 \pm 8	
-13	103 \pm 6	
-14	81 \pm 6	
-15	80 \pm 6	
-16	50 \pm 4	
-17	76 \pm 5	
-18	86 \pm 6	

Table 3: The measured partial fragmentation charge changing cross sections for 1 AGeV Si¹⁴⁺ and Fe²⁶⁺ ions on the CH₂ targets. The errors are statistical standard deviations. A systematic uncertainty of about 10% should be added.

- [2] J. W. Wilson et al., Health Phys. 68 (1995) 50.
- [3] U. Amaldi, Nucl. Phys. A751 (2005) 409.
- [4] S. Cecchini et al., Astrop. Phys. 1 (1993) 369 ; Nucl. Phys. A707 (2002) 513.
H. Dekhissi et al., Nucl. Phys. A662 (2000) 207.
- [5] W. R. Webber et al., Phys. Rev. C41 (1990) 520.
P. B. Price and Y. D. He, Phys. Rev. C43 (1991) 835.
S. E. Hirzebruch et al., Phys. Rev. C46 (1992) 1487; Nucl. Instr. Meth. B74 (1993) 519.
L. Sihver et al., Phys. Rev. C47 (1993) 1225.
Y. D. He and P. B. Price, Z. Phys. A348 (1994) 105.
L. Y. Geer et al., Phys. Rev. C52 (1995) 334.
G. Iancu et al., Radiat. Meas. 39 (2005) 525.
T. Toshito et al., Phys. Rev. C75 (2007) 054606.
- [6] C. Brechtmann et al., Z. Phys. A330 (1988) 407; Phys. Rev. C39 (1989) 2222.
- [7] C. Zeitlin et al., Phys. Rev. C56 (1997) 388.
- [8] F. Flesch et al., Radiat. Meas. 34 (2001) 237.
- [9] C. Zeitlin et al., Nucl. Phys. A784 (2007) 341.
- [10] A. N. Golovchenko et al., Nucl. Instr. Meth. B159 (1999) 233; Phys. Rev. C66 (2002) 014609.
- [11] G. Giacomelli et al., Nucl. Instr. Meth. A411 (1998) 41.
S. Cecchini et al., Radiat. Meas. 34 (2001) 55.
S. Balestra et al., Nucl. Instr. Meth. B254 (2007) 254.

- [12] S. Manzoor et al., Nucl. Phys. B Proc. Suppl. 172 (2007) 296.
G. Giacomelli et al., hep-ex/0702050.
- [13] M. Ambrosio et al., Eur. Phys. J. C25 (2002) 511.
- [14] T. Chiarusi et al., Radiat. Meas. 40 (2005) 424.
- [15] S. Manzoor et al., Nucl. Phys. B Proc. Suppl. 172 (2007) 92.
- [16] A. Noll et al., Nucl. Tracks Radiat. Meas. 15 (1988) 265.
- [17] H. L. Bradt, B. Peters, Phys. Rev. 77 (1950) 54.
- [18] S. Manzoor, Ph.D. Thesis, University of Bologna, Italy, and CIIT, Islamabad, Pakistan (2007).